Springer

Journal of
Mechanical
Science and
Technology

Journal of Mechanical Science and Technology 23 (2009) 3281~3291

www.springerlink.com/content/1738-494x
DOI 10.1007/s12206-009-1002-3

Analysis of tiltrotor whirl flutter in time and frequency domain †

Taeseong Kim[1], SangJoon Shin[1,*] and Taehyoun Kim[2]

[1]*Schoole of Mechanical and Aerospace Engineering, Institute of Advanced Aerospace Technology, Seoul National University, Seoul, 151-742, Korea*

[2]*Loads and Dynamics, Boeing Commercial Airplane Company, Seattle, WA, 98124-2207, USA*

(Manuscript Received March 4, 2009; Revised September 3. 2009; Accepted September 3, 2009)

Abstract

The whirl flutter phenomenon in a rotor is induced by in-plane hub forces, and imposes a serious limit on the forward speed. In this paper, based on Greenberg's model, quasi-steady and unsteady aerodynamic forces are formulated to examine the whirl flutter stability for a three-bladed rotor without flexible wing modes. Numerical results are obtained in both time and frequency domains. Generalized eigenvalue solution is utilized to estimate the whirl flutter stability in the frequency domain, and Runge-Kutta method is used to analyze it in time domain. The effects of varying the pylon spring stiffness and the swashplate geometric control coupling upon the flutter boundary are investigated. An optimum pitch-flap coupling parameter is discovered through the parametric study. Aeroelastic stability boundaries are estimated with the three different aerodynamic models. It is found that the analysis with the full unsteady aerodynamics predicts the highest flutter speed.

Keywords: Whirl flutter; Tiltrotor aircraft; Unsteady aerodynamics; Time domain; Frequency domain

1. Introduction

Since the phenomenon of whirl flutter was first discovered in the early 1960s, a number of investigations have been conducted because the whirl flutter instability, which is induced by excessive in-plane hub forces, imposes a serious limit on the forward speed in tiltrotor aircraft. This phenomenon has occurred in both turbo-prop and tiltrotor aircraft. The whirl flutter phenomenon in general aircraft with a propeller was first examined by Taylor and Brown [1]. However, a tiltrotor aircraft is more susceptible to this type of instability due to its higher level in the rotor blade flapping, bending, and the prominent control system flexibility.

Investigation of the whirl flutter instability is therefore required for tiltrotor aircraft for improvements in the forward flight performance, ride quality, and rotor component fatigue. Similarly, the fuselage vibration may be identified and alleviated through the investigation. However, to this date the phenomenon of dynamic instability has not been completely understood. Whirl flutter involves two modes of tiltrotor aircraft: a rotor and a pylon mode. The rotor mode is a backward whirl mode which occurs at low frequencies, while the pylon mode is a forward whirl mode whose frequency is close to the natural frequencies of the aircraft. Flutter frequencies of the pylon mode are higher than those associated with the rotor mode. There exists a significant difference between the two flutter mechanisms. In the pylon mode, the precession is in the same direction as the rotor blade rotation. In the other mode, the precession of the rotor mode is in the opposite direction. The whirl flutter instability occurs more frequently in the rotor mode because of its low resonance frequency [2, 3].

† This paper was recommended for publication in revised form by Associate Editor Hong Hee Yoo

*Corresponding author. Tel.: +82 2 880 1642, Fax.: +82 2 887 2662
E-mail address: ssjoon@snu.ac.kr

The whirl flutter does not occur at a low inflow flight condition; it happens at a high inflow condition, such as during a high speed cruise flight. The aerodynamic forces and moments of the rotor blade are generated proportional to the change of local angle of attack on each blade element. It causes a precession of the rotor blade, which in turn provides the mechanism for the dynamic instability. The mechanism of the whirl flutter is illustrated in Fig. 1 for a two-bladed rotor. Under a high inflow flight condition, the angle of attack increment at a representative 75% spanwise location, $\Delta\alpha$, is negative at Blade No. 1 instantaneously. The lift increment, ΔL, appears perpendicular to the control plane. This lift component is divided into a change of thrust, ΔT, and an H-force, ΔH. Precession of the rotor blade is created by the H-force components both in Blade Nos. 1 and 2, because these forces act in the same direction. At the same time, high transient flapping is caused by the thrust component, ΔT, because these forces act in the opposite directions. These incremental aerodynamic forces and moments cause the whirl flutter instability at a certain flight speed [2].

To increase the whirl flutter stability boundary, Hall examined the effect of varying the pitch-flap coupling and the pylon stiffness parameters [2]. Stability of the proprotor pylon was affected to a certain degree by such methodologies. The rotor blade design was also modified to increase the stability speed margin by Acree et al. [4]. In Ref. [5], higher harmonic control (HHC) was experimentally employed at both the rotor swashplate and the wing flaperon to reduce vibrations induced in an airplane mode. The effectiveness of the swashplate and the wing flaperon acting either in a single or combination mode was demonstrated in reducing the 1 per revolution (/rev) and 3/rev vibration. In the 1990's generalized predictive

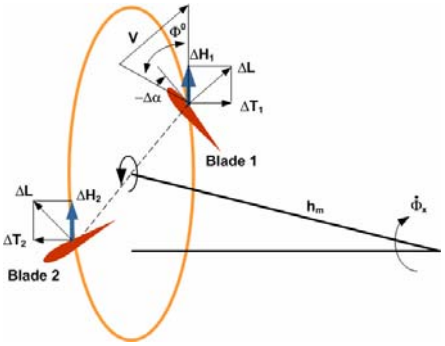

Fig. 1. Mechanism of the whirl flutter.

control (GPC), which is a digital time domain multi-input multi-output predictive control method, was experimentally investigated to evaluate the effectiveness of an adaptive control algorithm. Active control was introduced into the non-rotating swashplate using three high-frequency servo-controlled hydraulic actuators mounted aft of the swashplate inside the pylon fairing [3, 6]. The GPC algorithm was highly effective in improving the stability in the critical wing mode tested. However, it was not an attractive option due to the complexity of the algorithm. More recently, another active control algorithm employed via actuation of the wing flaperon and the rotor swashplate was examined for whirl flutter stability and robustness augmentation [7]. Full state feedback, which was composed of linear quadratic regulator (LQR) optimal control and wing state feedback control, was used in that investigation.

From the survey described above, most of the previous analytical investigations relied on quasi-steady aerodynamic approximations ignoring the fully unsteady characteristics in the aerodynamics. A relevant formulation for unsteady aerodynamics needs to be included to represent more realistic aerodynamic environment generated in tiltrotor aircraft. By including an unsteady aerodynamic effect, it is possible to establish a more complete analytical model which is expected to yield a better flutter prediction. An immediate objective of the present paper is to develop an analytical model with an unsteady aerodynamic formulation and validate it against the other analytical or experimental results. On the other hand, a comprehensive analysis code, such as CAMRAD or DYMORE, usually involves a considerable amount of the computational resources, although it gives more accurate estimate results. For general aeroelastic problems, such as stability and response analysis of a fixed or rotary wing aircraft, it is still useful to obtain an approximate solution quickly using a simple simulation model. The present paper aims to provide an efficient model to conduct a tiltrotor aeroelastic stability analysis. It is constructed with a simple aeroelastic model including the effect of the unsteady aerodynamics.

In this paper, a gimbaled stiff in-plane three-bladed rotor system is used to investigate its whirl flutter stability. An analytical model on passive control methodologies for whirl flutter stability in tiltrotor aircraft is also developed. Numerical results are obtained and presented in time and frequency domain. Gener-

alized eigenvalue solution is used to estimate whirl flutter instability in frequency domain, while the Runge-Kutta method is used to analyze in time domain.

2. Description of the model

2.1 Structural dynamics model

The structural model, which is shown in Fig. 2, is developed based on the formulation used in Ref. 8. The present model consists of four degrees of freedom: two rotor blade flapping angles (β_{1C} and β_{1S}), and pitch and yaw angles (α_y and α_x) of the pylon. Positive direction of the flapping motion is defined for forward displacement of the blade tip from the disk plane. Positive direction of the pitch angle for the pylon and yaw are defined for upward and left rotation of the hub, respectively. A flapping motion of the rotor is assumed to be composed of the totally rigid blades.

Using the force and moment equilibrium, the equations of the structural inertia, damping, and stiffness are obtained as follows.

$$I_b\left(\ddot{\beta}_m + \nu_\beta^2 \beta_m - \left(\ddot{\alpha}_y - 2\Omega\dot{\alpha}_x\right)\cos\psi_m + \left(\ddot{\alpha}_x + 2\Omega\dot{\alpha}_y\right)\sin\psi_m\right) = M_{F_m} \quad (1)$$

$$I_x\ddot{\alpha}_x + C_x\dot{\alpha}_x + K_x\alpha_x = M_x - h_m Y \quad (2)$$

$$I_y\ddot{\alpha}_y + C_y\dot{\alpha}_y + K_y\alpha_y = M_y + h_m H \quad (3)$$

Eqs. (1), (2), and (3) represent, respectively, the flap, yaw, and pitch moment equilibrium. Employing the Fourier transformation to Eq. (1) only, it is possible to convert these into the equations in a non-rotating frame. These equations are non-dimensionalized with ρ, Ω, R, I_b, γ, σ, and $I_b(N/2)$. The equations of motion for the four degrees of freedom can be represented in a matrix form as in Eq. (4).

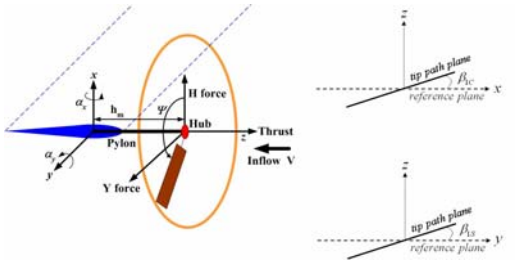

Fig. 2. A completely rigid-bladed rotor system.

$$\begin{bmatrix} 1 & 0 & -1 & 0 \\ 0 & 1 & 0 & 1 \\ 0 & 0 & I_y^* & 0 \\ 0 & 0 & 0 & I_x^* \end{bmatrix} \begin{pmatrix} \beta_{1C}'' \\ \beta_{1S}'' \\ \alpha_y'' \\ \alpha_x'' \end{pmatrix} + \begin{bmatrix} 0 & 2 & 0 & 2 \\ -2 & 0 & 2 & 0 \\ 0 & 0 & C_y^* & 0 \\ 0 & 0 & 0 & C_x^* \end{bmatrix} \begin{pmatrix} \beta_{1C}' \\ \beta_{1S}' \\ \alpha_y' \\ \alpha_x' \end{pmatrix} + \begin{bmatrix} \nu_\beta^2 - 1 & 0 & 0 & 0 \\ 0 & \nu_\beta^2 - 1 & 0 & 0 \\ 0 & 0 & K_y^* & 0 \\ 0 & 0 & 0 & K_x^* \end{bmatrix} \begin{pmatrix} \beta_{1C} \\ \beta_{1S} \\ \alpha_y \\ \alpha_x \end{pmatrix} = \gamma \begin{pmatrix} M_{F_{1C}}/ac \\ M_{F_{1S}}/ac \\ 2C_{M_y}/\sigma a + h_m(2C_H/\sigma a) \\ 2C_{M_x}/\sigma a - h_m(2C_y/\sigma a) \end{pmatrix} \quad (4)$$

The structural dynamics part is organized in the left hand side (LHS) in Eq. (4), while the aerodynamics part is in the right hand side (RHS) of the same equation.

2.2 Aerodynamic model

The rotor is assumed to be operating in a purely axial flow in equilibrium. When evaluating the blade forces and moments, each velocity component consists of a trim and a perturbation component. Trim state is assumed to be established already and the perturbation from it is considered for the flutter analysis.

The rotor aerodynamic forces and moments are defined on the RHS of Eq. (4). Three different aerodynamic models are used to predict the whirl flutter stability both in time and frequency domains. They consist of two quasi-steady and an unsteady aerodynamic models. The first aerodynamic model is widely used and is quoted as a normal quasi-steady aerodynamics in this paper. This aerodynamic model is developed based on Ref. 8, and is described in Eq. (5) below. The second quasi-steady aerodynamic model is presented in Eq. (6). It is equivalent to replacing $C(k)$ by 1 in Greenberg's aerodynamic model [9, 10]. In Eq. (6), the noncirculatory part is ignored because most of its terms are eliminated by the coordinate transformation and the effects of the remaining terms are very small [11]. This model is quoted as Greenberg's quasi-steady aerodynamics in this paper. For a full unsteady aerodynamic representation, Greenberg's two-dimensional unsteady aerodynamic model, which is extended to account for time-varying incoming airspeed, is used and its expression is pre-

sented in Eq. (7) [10, 12].

$$L = 2\pi\rho U(t)^2 b\alpha(t) \tag{5}$$

$$L = 2\pi\rho U(t)b\Big[(\dot{h}(t)+U(t)\theta(t)) + b(0.5-a_h)\dot{\theta}(t)_{ref}\Big] \tag{6}$$

$$\begin{aligned} L &= 2\pi\rho U(t)bC(k)[(\dot{h}(t)+U(t)\theta(t)) + b(\frac{1}{2}-a_h)\dot{\theta}(t)_{ref}] + \pi\rho b^2[\ddot{h}(t)+\dot{U}(t)\theta(t) \\ &\quad + U(t)\dot{\theta}(t) - ba_h\ddot{\theta}(t)_{ref}] \\ &= Circulatory\ part(L_C) + Noncirculatory\ part(L_{NC}) \end{aligned} \tag{7}$$

The aerodynamic environment of the rotor blade typical section is shown in Fig. 3. All the velocities and forces are estimated with respect to the hub plane, which is used as a reference frame. The aerodynamic forces on the blade typical section are lift (L), and drag (D).

According to Fig. 3, the total forces in x and z direction can be obtained as follows.

$$\frac{\bar{F}_z}{a\bar{c}} = \frac{\bar{L}}{a\bar{c}}\cos\phi - \frac{\bar{D}}{a\bar{c}}\sin\phi \tag{8}$$

$$\frac{\bar{F}_x}{a\bar{c}} = \frac{\bar{L}}{a\bar{c}}\sin\phi + \frac{\bar{D}}{a\bar{c}}\cos\phi \tag{9}$$

where, using a small angle approximation, $\sin\phi = u_P(\psi)/U(\psi)$, and $\bar{L}$ and $\bar{D}$ are the modified forms of L and D, which are non-dimensionalized by $\rho\Omega^2R^3$.

In Ref. 8, it was found that the aerodynamic forces acting on a blade are dominated by the lift in a rotor flow field at a high inflow. Thus, the drag forces are not included and only the $c_{l\alpha}$ terms are retained. Then Eqs. (8) and (9) can be simplified as follows.

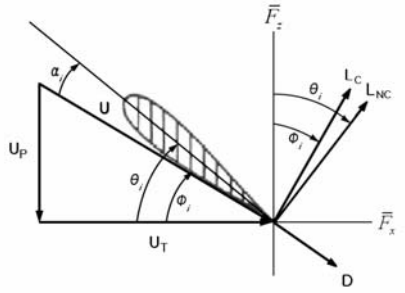

Fig. 3. Resultant and inflow velocities on the blade typical section.

$$\frac{\bar{F}_z}{a\bar{c}} = \frac{\bar{L}}{a\bar{c}}\frac{u_T(\psi)}{U(\psi)} \tag{10}$$

$$\frac{\bar{F}_x}{a\bar{c}} = \frac{\bar{L}}{a\bar{c}}\frac{u_P(\psi)}{U(\psi)} \tag{11}$$

$$\frac{\bar{F}_r}{a\bar{c}} = \overline{Uu}_R\frac{C_d}{2a} - \beta\frac{\bar{F}_z}{a\bar{c}} \simeq -\beta\frac{\bar{F}_z}{a\bar{c}} \tag{12}$$

The above expressions can be used for the two quasi-steady aerodynamic models. However, it is not possible to obtain the forces and moments by using the above expressions in the full unsteady aerodynamic model because there exist two parts in the expression, the noncirculatory and circulatory parts. Those parts are included in Eq. (7). The lift deficiency function, $C(k)$, can be represented only in frequency domain as in Eq. (7). Therefore, to convert the frequency-valued aerodynamics to time domain Jones' rational approximation is utilized as follows [13, 14].

$$C(s) = \left[\frac{0.5\bar{s}^2 + 0.2808\bar{s} + 0.01365}{\bar{s}^2 + 0.3455\bar{s} + 0.01365}\right] \tag{13}$$

where $\bar{s} = s(\bar{b}R/U_0)$.

By substituting Eq. (13) into Eq. (7), a state space equation is thus obtained:

$$\begin{aligned} \begin{Bmatrix}\dot{X}_1\\ \dot{X}_2\end{Bmatrix} &= \begin{bmatrix}a_{11} & a_{12}\\ 1 & 0\end{bmatrix}\begin{Bmatrix}X_1\\ X_2\end{Bmatrix} + \begin{Bmatrix}1\\ 0\end{Bmatrix}Q(t) \\ y &= \begin{bmatrix}C & D\end{bmatrix}\begin{Bmatrix}X_1\\ X_2\end{Bmatrix} + 0.5Q(t) \end{aligned} \tag{14}$$

where, $Q(t) = (\dot{h}(t)+U(t)\alpha(t)) + b(0.5-a_h)\dot{\theta}(t)_{ref}$, $a_{11} = -0.3455(U_0/\bar{b}R)$, $a_{12} = -0.0137(U_0/\bar{b}R)^2$, $C = 0.1081(U_0/\bar{b}R)$, and $D = 0.0068(U_0/\bar{b}R)^2$.

From Eq. (14), new state space equations for the augmented state variables and the circulatory part of the lift can be formulated:

$$\begin{aligned} \begin{Bmatrix}\bar{X}_1'\\ \bar{X}_2'\end{Bmatrix} &= \begin{bmatrix}a_{11} & a_{12}\\ 1 & 0\end{bmatrix}\begin{Bmatrix}\bar{X}_1\\ \bar{X}_2\end{Bmatrix} + \begin{Bmatrix}1\\ 0\end{Bmatrix}Q(\psi) \\ \bar{L}_c &= 2\pi bU(\psi)\left\{C\bar{X}_1 + D\bar{X}_2 + 0.5Q(\psi)\right\} \end{aligned} \tag{15}$$

where, $X_1 = R\bar{X}_1$, $X_2 = (R/\Omega)\bar{X}_2$, and $\partial/\partial t = \Omega(\partial/\partial\psi)$.

Eq. (15) can be used to replace the circulatory part

in Eq. (7). Therefore, an updated lift expression is obtained:

$$\bar{L} = \underbrace{2\pi \bar{b} U(\psi)\left\{C\bar{X}_1 + D\bar{X}_2 + 0.5Q(\psi)\right\}}_{\bar{L}_C} \tag{16}$$

In Eq. (16), the augmented state variables, $\bar{X}_1$ and $\bar{X}_2$, are governed by a system of ordinary differential equations, and associated with a downwash velocity at the three quarter chord location, $Q(\psi)$, [15]. These augmented states are driven by the time history of $Q(\psi)$ at each spanwise location. However, in this paper the augmented state variables of the typical section at ¾ span location are utilized as an averaged value. A Fourier coordinate transformation may be applied to express $Q(\psi)$, $\bar{X}_1$, and $\bar{X}_2$ in the non-rotating coordinate system:

$$\begin{aligned} Q(\psi) &= \bar{Q}_0 + \sum_{n=1}^{NH} \bar{Q}_{1cn}\cos n\psi + \bar{Q}_{1sn}\sin n\psi \\ \bar{X}_1 &= \bar{X}_{1_0} + \sum_{n=1}^{NH} \bar{X}_{1cn}\cos n\psi + \bar{X}_{1sn}\sin n\psi \\ \bar{X}_2 &= \bar{X}_{2_0} + \sum_{n=1}^{NH} \bar{X}_{2cn}\cos n\psi + \bar{X}_{2sn}\sin n\psi \end{aligned} \tag{17}$$

where *NH* is the number of harmonics retained in the Fourier analysis.

By substituting Eq. (17) into Eq. (16), it is possible to obtain the lift expression in the full unsteady aerodynamic model in time domain. According to Fig. 3, the total forces in each direction are obtained as in Eqs. (10) and (11).

Fig. 4 shows the in-plane forces, which are *H* and *Y* forces on each blade.

From Fig. 4, the in-plane forces can be expressed as follows.

$$\begin{aligned} H &= F_x \sin\psi_m + F_r \cos\psi_m \\ Y &= -F_x \cos\psi_m + F_r \sin\psi_m \end{aligned} \tag{18}$$

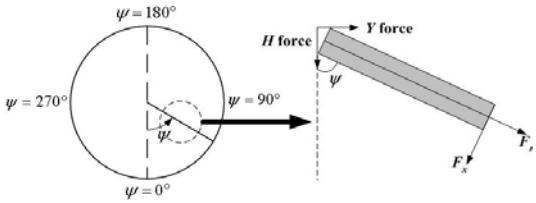

Fig. 4. In-plane *H* and *Y* force on the blade.

The net rotor aerodynamic forces and moments are obtained by integrating the sectional forces and moments over the span of the blade and summing over all three blades.

$$\begin{aligned} \frac{C_T}{\sigma a} &= \frac{1}{N}\sum_m \int_0^1 \frac{\bar{F}_z}{a\bar{c}} d\bar{r} \\ \frac{2C_H}{\sigma a} &= \frac{2}{N}\sum_m (\cos\psi_m \int_0^1 \frac{\bar{F}_r}{a\bar{c}} d\bar{r} + \sin\psi_m \int_0^1 \frac{\bar{F}_x}{a\bar{c}} d\bar{r}) \\ \frac{2C_Y}{\sigma a} &= \frac{2}{N}\sum_m (\sin\psi_m \int_0^1 \frac{\bar{F}_r}{a\bar{c}} d\bar{r} - \cos\psi_m \int_0^1 \frac{\bar{F}_x}{a\bar{c}} d\bar{r}) \\ \frac{\bar{M}_F}{ac} &= \int_0^1 \bar{r}\frac{\bar{F}_z}{a\bar{c}} d\bar{r} \end{aligned} \tag{19}$$

The pitch and yaw moments of the hub due to the rotor are to be formulated. The source of the hub moment is the bending moment at the blade rotor due to the flapping, $M_m = I_b(\nu_\beta^2 - 1)\beta_m$. Therefore, the rotor lateral and longitudinal moment coefficients are formulated as follows.

$$\frac{2C_{My}}{\sigma a} = -\frac{\nu_\beta^2 - 1}{\gamma}\beta_{1c} \tag{20}$$

$$\frac{2C_{Mx}}{\sigma a} = \frac{\nu_\beta^2 - 1}{\gamma}\beta_{1s} \tag{21}$$

2.3 Governing equations

Once the rotor forces and moments are obtained as in Eqs. (19), (20), and (21), they need to be substituted into the RHS in Eq. (4). The governing equation of motion is then obtained for the four degree-of-freedom system. Since the governing equations for the normal quasi-steady and Greenberg's quasi-steady aerodynamic models result in the same form, only two types of governing equations are needed.

2.3.1 Quasi-steady aerodynamic models

Putting the forces and moments of the rotor, which are expressed in Eqs. (19), (20) and (21) with Eqs. (5) and (6), into the RHS of Eq. (4) gives the following expression:

$$RHS = C_a y' + K_a y + G_a p + Z_a g \tag{22}$$

where, $y^T = \{\beta_{1c} \quad \beta_{1c} \quad \alpha_y \quad \alpha_x\}$, $p^T = \{\theta_{1C} \quad \theta_{1S}\}$, $g^T = \{\beta_G \quad \alpha_G\}$ and the subscript *a* means an aerodynamic part.

The governing equation can be obtained as follows:

$$M_s y'' + C_s y' + K_s y = C_a y' + K_a y + G_a p + Z_a g \quad (23)$$

where the subscript s means a structural part and all the elements of the matrices are dimensionless quantities.

For simplicity, Eq. (23) can be rearranged as

$$\begin{aligned} M_s y'' &= -(C_s - C_a)y' - (K_s - K_a)y + G_a p + Z_a g \\ \therefore y'' &= -M_s^{-1}(C_s - C_a)y' - M_s^{-1}(K_s - K_a)y \\ &\quad + M_s^{-1}G_a p + M_s^{-1}Z_a g \\ &= -(M_s^{-1}\bar{C})y' - (M_s^{-1}\bar{K})y + M_s^{-1}G_a p \\ &\quad + M_s^{-1}Z_a g \\ &= -Ay' - By + \bar{G}p + \bar{Z}g \end{aligned} \quad (24)$$

where, $\bar{C} = (C_s - C_a)$, $\bar{K} = (K_s - K_a)$, $A = (M_s^{-1}\bar{C})$, $B = (M_s^{-1}\bar{K})$, $\bar{G} = (M_s^{-1}G_a)$, and $\bar{Z} = (M_s^{-1}Z_a)$.

Converting Eq. (24) into a state space form gives

$$Y' = \underbrace{\begin{bmatrix} 0 & I \\ -B & -A \end{bmatrix}}_{8\times8} \underbrace{\begin{Bmatrix} y \\ y' \end{Bmatrix}}_{8\times1} + \underbrace{\begin{bmatrix} 0 & 0 \\ \bar{G} & \bar{Z} \end{bmatrix}}_{8\times4} \underbrace{\begin{Bmatrix} p \\ g \end{Bmatrix}}_{4\times1} \quad (25)$$

where $Y^T \equiv \{ y \quad y' \}$.

2.3.2 Full unsteady aerodynamic model

The method for deriving the governing equation for this case is similar to that for the quasi-steady aerodynamic models. However, the present governing equation needs to include an ordinary differential equation for the augmented state variables, in addition to Eq. (4).

Substituting the rotor forces and moment, which are obtained at the hub frame, into the aerodynamic part in Eq. (4), a state space equation is obtained as follows.

$$Y' = \underbrace{\begin{bmatrix} 0 & I \\ -B & -A \end{bmatrix}}_{8\times8} \underbrace{\begin{Bmatrix} y \\ y' \end{Bmatrix}}_{8\times1} + \underbrace{\begin{Bmatrix} 0 \\ C \end{Bmatrix}}_{8\times4} \underbrace{X}_{4\times1} + \underbrace{\begin{bmatrix} 0 & 0 \\ \bar{G} & \bar{Z} \end{bmatrix}}_{8\times4} \underbrace{\begin{Bmatrix} p \\ g \end{Bmatrix}}_{4\times1} \quad (26)$$

where, $X^T = \left(\bar{X}_{1_C} \quad \bar{X}_{1_S} \quad \bar{X}_{2_C} \quad \bar{X}_{2_S} \right)$.

Eqs. (26) and (15) can be simplified as

$$\begin{aligned} Y' &= \underbrace{T^*}_{8\times8}\underbrace{Y}_{8\times1} + \underbrace{S^*}_{8\times4}\underbrace{X}_{4\times1} + \underbrace{O^*}_{8\times4}\underbrace{v}_{4\times1} \\ X' &= \underbrace{E}_{4\times4}\underbrace{X}_{4\times1} + \underbrace{D}_{4\times8}\underbrace{Y}_{8\times1} \end{aligned} \quad (27)$$

where, $T^* = \underbrace{\begin{bmatrix} 0 & I \\ -B & -A \end{bmatrix}}_{8\times8}$, $S^* = \underbrace{\begin{Bmatrix} 0 \\ C \end{Bmatrix}}_{8\times4}$, $\mathrm{O}^* = \underbrace{\begin{bmatrix} 0 & 0 \\ \bar{G} & \bar{Z} \end{bmatrix}}_{8\times4}$,

$E = \underbrace{\begin{bmatrix} a_{11} & a_{12} \\ 1 & 0 \end{bmatrix}}_{8\times8}$, $D = \underbrace{\begin{Bmatrix} q \\ 0 \end{Bmatrix}}_{4\times8}$, $v = \underbrace{\begin{Bmatrix} p \\ g \end{Bmatrix}}_{4\times1}$, $A = (\bar{M}^{-1}\bar{C})$,

$B = (\bar{M}^{-1}\bar{K})$, $C = (\bar{M}^{-1}Z_a)$, $\bar{M} = (M_s - M_a)$,

$\bar{C} = (C_s - C_a)$, $\bar{K} = (K_s - K_a)$, $\bar{G} = (M_s^{-1}G_a)$,

$\bar{Z} = (M_s^{-1}Z_a)$ and q are elements of $\bar{Q}_{1c}$ and $\bar{Q}_{1s}$.

Combining the two parts in Eq. (27), the following governing equation, which enables an analysis both in time and frequency domain, is obtained in a state space form:

$$\underbrace{\begin{bmatrix} Y' \\ X' \end{bmatrix}}_{12\times1} = \underbrace{\begin{bmatrix} \underbrace{T^*}_{8\times8} & \underbrace{S^*}_{8\times4} \\ \underbrace{D}_{4\times8} & \underbrace{E}_{4\times4} \end{bmatrix}}_{12\times12} \underbrace{\begin{bmatrix} Y \\ X \end{bmatrix}}_{12\times1} + \underbrace{\begin{bmatrix} \underbrace{O^*}_{8\times4} \\ \underbrace{0}_{4\times4} \end{bmatrix}}_{12\times4} \underbrace{\begin{bmatrix} p \\ g \end{bmatrix}}_{4\times1} \quad (28)$$

where all the elements of the matrices are dimensionless quantities.

3. Numerical results

Numerical investigation is conducted to obtain the whirl flutter stability boundary in time and frequency domain using the various aerodynamic models presented above. Two passive control algorithms, including variations of the pylon stiffness and the pitch-flap coupling, are examined to improve the whirl flutter stability boundary.

It is assumed that the aircraft has reached a trim state; therefore, only the perturbation effects are considered to obtain the results regarding the whirl flutter stability. The perturbation velocities are defined as follows:

$$\delta U = \frac{u_{T_0}}{U_0}\delta u_T + \frac{u_{p_0}}{U_0}\delta u_p \quad (29)$$

where, $\delta u_p = r(\dot{\beta} - \dot{\alpha}_y \cos\psi_m + \dot{\alpha}_x \sin\psi_m) + Vu_G$ $= r\delta u_{p_B} + Vu_G$ and $\delta u_T = -h_m(\dot{\alpha}_y \sin\psi_m + \dot{\alpha}_x \cos\psi_m)$ $+(V + v)(\alpha_y \sin\psi_m + \alpha_x \cos\psi_m) + V(\beta_G \cos\psi_m$ $+\alpha_G \sin\psi_m)$

To investigate the whirl flutter instability, the aircraft flight speed is arbitrarily increased and its

stability is evaluated while keeping the same structural parameters, $h_m = 0.261$, $\gamma = 3.83$, $\nu_\beta = 1.02$, $\xi = 0.04$, $\Omega = 458 RPM$, and $b = 0.047$, of all which are dimensionless quantities. Since the perturbations in control pitch input and gust are not considered in the present analysis, $\bar{G}$, $\bar{Z}$, and O^* matrices are ignored in Eqs. (25) and (28). All the structural and aerodynamic quantities used in this paper are dimensionless values. The numerical values on the structural parameters used in this investigation are borrowed from Ref. 8.

3.1 Normal quasi-steady aerodynamic model

This section presents the results using the normal quasi-steady aerodynamic model in which the lift is represented by Eq. (5). Fig. 5 illustrates the results of the stability analysis in time and frequency domains for the aircraft speed range of 84-93 m/sec. Fig. 5(a) shows the result of the time domain analysis for three different speeds. The system remains stable until 90 m/sec; however, the aircraft becomes unstable when its flight speed is increased to 93 m/sec. Fig. 5(b) is the result of the frequency domain analysis for the same flight speed range. When the system poles are located on the imaginary axis, the system is on the verge of flutter stability. If they are located in the right half plane, the system is unstable. Again, it is observed that the stability boundary is approximately 90 m/sec, which is considered to be a conservative whirl flutter boundary for the present tiltrotor aircraft.

Passive control algorithms such as variations of the pylon stiffness and the pitch-flap coupling (δ_3) are applied. Fig. 6 shows the result of the pylon stiffness variation in time domain. As can be seen, the flutter stability is improved by increasing the pylon stiffness. The flutter boundary is almost linearly increased by the increment of the pylon stiffness until 20% relative to the nominal value. Fig. 7 shows improvements in whirl flutter stability for the pitch-flap coupling from -15 to 30° in the rotor system. Pitch-flap coupling is one of the important parameters for the tiltrotor aircraft design. Positive pitch-flap coupling, which is defined as a blade flapping up producing a blade pitching up, is represented by a negative δ_3 in the governing equation. Fig. 7 shows that both positive and negative δ_3 are influential upon the stability. However there is an effective range of the pitch-flap coupling which may improve the flutter stability. In the present aerodynamic model, an optimum

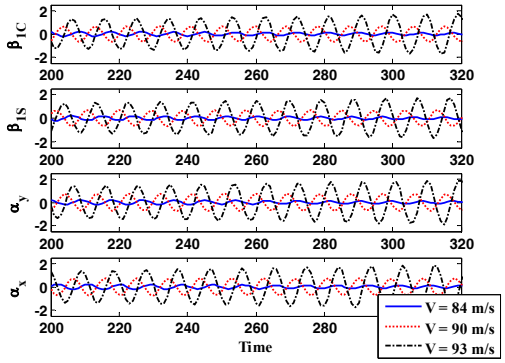

(a)

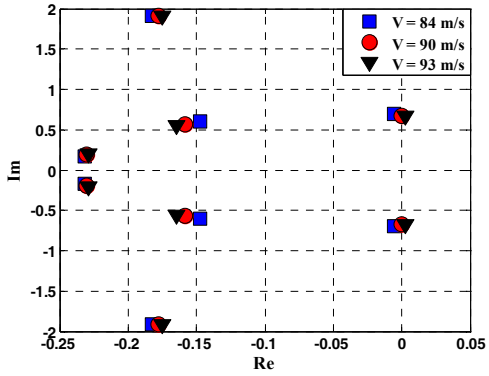

(b)

Fig. 5. Time and frequency domain results using the normal quasi-steady aerodynamics.

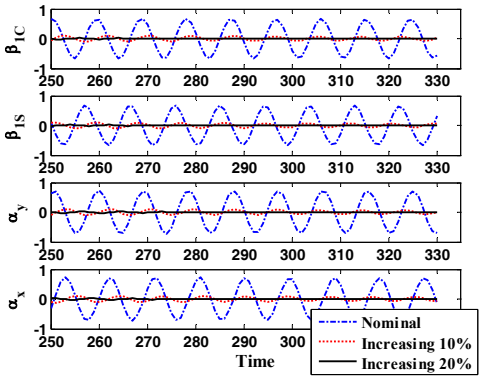

Fig. 6. Results with respect to the pylon stiffness at V=90(m/sec).

pitch-flap coupling angle is found to be approximately 10°. When it is smaller or larger than 10°, the system poles are closely located to an imaginary axis, signifying a reduction in the dynamic stability.

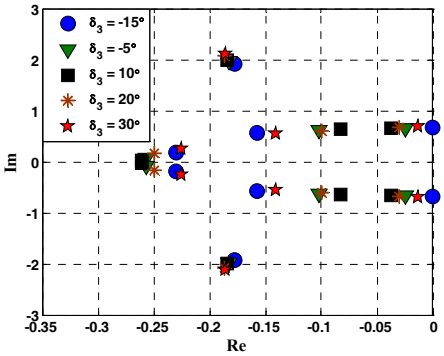

Fig. 7. Results with respect to δ_3 at V=90(m/sec).

3.2 Greenberg's quasi-steady aerodynamic model

Greenberg's quasi-steady aerodynamic model has a similar formulation with that for the previous normal quasi-steady aerodynamics. However, the lift formulation has extra rate. According to Eq. (6), a few first-order time derivative terms, which are $\dot{h}$ and $\dot{\theta}_{ref}$, are newly included in the present Greenberg quasi-steady aerodynamics. Here, $\dot{h}$ is a velocity of the flapping motion, which is due to $-\delta u_P$, and $\dot{\theta}_{ref}$ is an angular velocity of the pitching motion with respect to an inertial frame.

Only the first-order perturbation terms are considered as it is done in the previous normal quasi-steady aerodynamics. Then, the perturbation term of θ_{ref} is organized as follows.

$$\delta\theta_{ref} = -K_p\beta + \alpha_y \cos\psi + \alpha_x \sin\psi \tag{30}$$

Substituting Eqs. (29)-(30) into (7), the lift formulation can be obtained, and then all the forces and moments acting at a hub are expressed in the hub reference frame.

Fig. 8 shows the results of the whirl flutter stability in time and frequency domain using Greenberg's quasi-steady aerodynamics. According to the time domain analysis, as in Fig. 8(a), the flutter boundary is found to be 89 m/sec. Frequency domain analysis provides the same result, as in Fig. 8(b). When the flight speed is 89 m/sec, the system poles are located on the imaginary axis. There is a slight difference regarding the flutter boundary between the normal and Greenberg's aerodynamic models. Under the present Greenberg quasi-steady aerodynamics, flutter occurs slightly earlier than it does under the normal quasi-steady one.

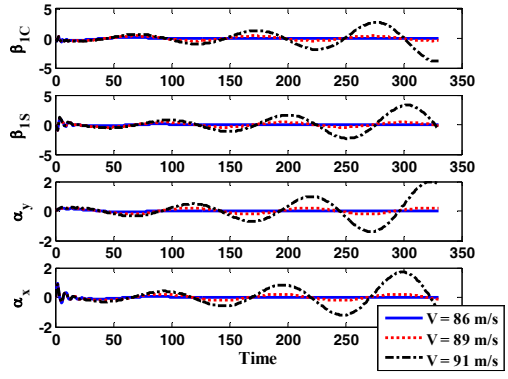

(a)

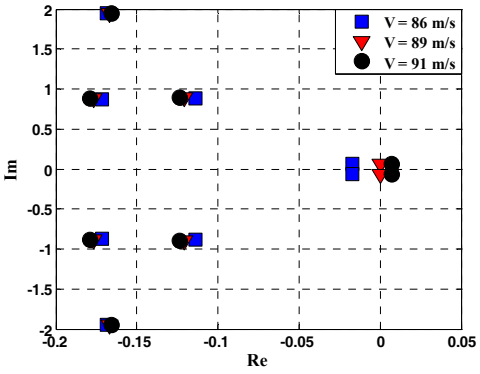

(b)

Fig. 8. Time and frequency domain results using Greenberg's quasi-steady aerodynamics.

3.3 Full unsteady aerodynamic model

As mentioned previously, a quasi-steady aerodynamic model is generally not capable of describing a realistic aerodynamic environment occurring in tiltrotor aircraft. In this section, numerical investigation is presented using Greenberg's two-dimensional unsteady aerodynamic model. The difference between Greenberg's quasi-steady and the full unsteady aerodynamics is the addition of the lift deficiency function in the latter model.

Fig. 9 illustrates the time and frequency results for the flight speed from 106 to 110 m/sec. According to Fig. 9(a) and (b), the stability boundary is found to be 109 m/sec based on the full unsteady aerodynamics. Thus, the critical flight speed at which an instability occurs is predicted to be the highest under the full unsteady aerodynamics.

Fig. 10 shows the result when varying the pylon stiffness under the full unsteady aerodynamics. The nominal flutter speed is based on the results in Fig. 9.

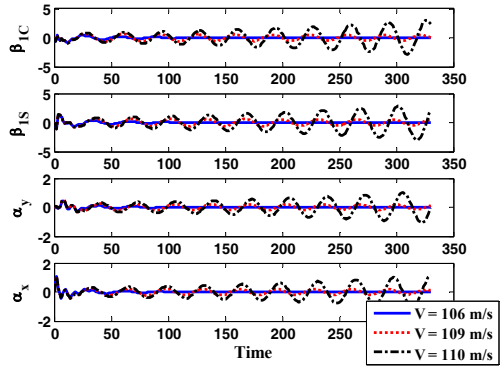

(a)

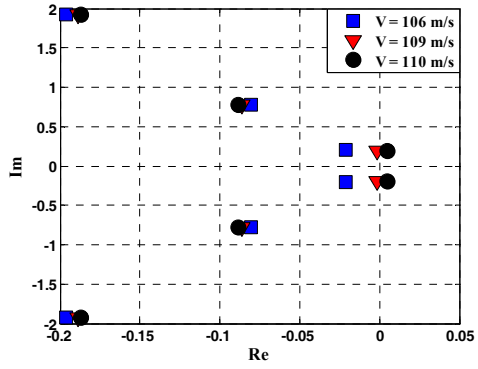

(b)

Fig. 9. Time and frequency domain results using the full unsteady aerodynamics.

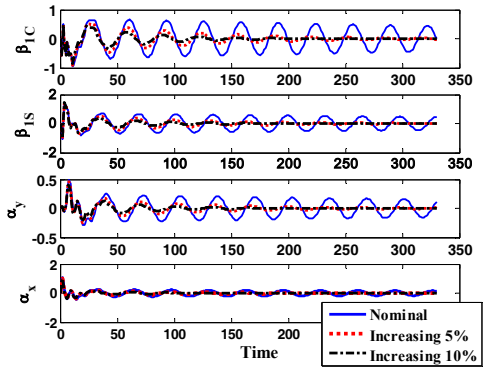

Fig. 10. Results with respect to the pylon stiffness based on full unsteady aerodynamics.

It is apparent that the whirl flutter boundary is proportionally improved when numerically increasing the pylon stiffness until approximately 10% relative to its nominal value.

Fig. 11 shows a comparison of the whirl flutter stability in time domain among the three aerodynamic models used. The whirl flutter stability predicted by the full unsteady aerodynamic model is higher than the result from the normal quasi-steady aerodynamic model is, by approximately 20%. Between the normal and Greenberg's quasi-steady aerodynamic model, the stability boundary is underestimated by approximately 1% by the latter.

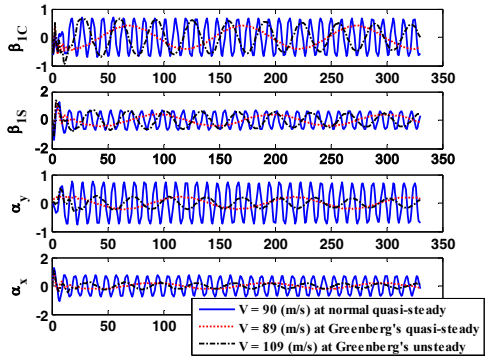

Fig. 11. Time domain results at the respective flutter condition by each aerodynamic model.

Table 1. Comparison results for the flutter stability boundary.

Analytical model	Flutter speed
Present model	109 m/sec (215 kts)
Johnson [16]	155 m/sec (305 kts)
Nixon [17]	146 m/sec (285 kts)
Hathaway [18]	154 m/sec (302 kts)
XV-15 [19]	153 m/sec (300 kts)

3.4 Comparison with other analysis results

The whirl flutter stability analysis result based on the full unsteady aerodynamic model is compared with the other existing analytical results and the full-scale XV-15 aircraft flight test data. Table 1 shows the whirl flutter stability boundaries obtained from those cases.

The flutter stability boundary is predicted to be approximately 150 m/sec by most of the analyses, while the whirl flutter occurs at 109 m/sec according to the present model. Inclusion of the elastic wing mode is believed to make such a significant discrepancy (approximately 28% difference). Johnson's and Nixon's analytical models use a sophisticated elastic beam model for the rotor blade and wing. Hathaway's model uses a rigid blade with a blade flap and lag degree of freedom, control system flexibility, and elastic wing. However, the present analysis is based on a

rigid-bladed rotor and pylon. The present analysis does not include the elastic wing representation, which suggests that the present analysis model needs to be upgraded to a more sophisticated one for a better flutter stability prediction. However, the present propeller/nacelle flutter analysis is useful for the design purpose, although it is less sophisticated. Furthermore, the present analysis is capable of including the unsteady aerodynamic effect. A more conservative flutter boundary can be predicted with a simple rigid blade structural model, while the other existing analytical results are based on only quasi-steady aerodynamics.

4. Conclusions and future works

Time and frequency domain analyses are conducted using a newly developed analytical model on passive control methodologies for whirl flutter stability in tiltrotor aircraft. The following conclusions are drawn from the present study.

(1) A simple and fast simulation framework is developed, including an unsteady aerodynamic force for the rotor in tiltrotor aircraft. It is a first attempt to consider an unsteady aerodynamic effect in a tiltrotor aeroelastic stability analysis.

(2) The two quasi-steady aerodynamics models predict the whirl flutter stability boundary at almost the same flight speed.

(3) The full unsteady aerodynamic theory predicts the whirl flutter instability to occur at a higher flight velocity than quasi-steady aerodynamic models do. Also, a comparison with the other analytical models, which includes the three-dimensional elastic blade motion and elastic wing mode, shows a discrepancy in the flutter stability boundary. Such discrepancy can be attributed to the fact that the present analysis consists of a propeller/nacelle model in which only the flapping motion of a rigid rotor blade is considered. However, other analyses consist of a propeller/nacelle/wing model in which the flap and lag motion of the rotor and the elastic wing motion are utilized.

(4) Passive control algorithms, which consider varying the pylon stiffness and the pitch-flap coupling, are found to improve the whirl flutter stability boundary. It is found that each system has an optimum pitch-flap coupling value. Also, its stability boundary is linearly increased in proportion to the pylon stiffness. The stability results by the quasi-steady aerodynamics are found to be more conservative than those obtained by the full unsteady aerodynamic model.

In the future, the effects of the blade lead-lag motion and elastic wing will be added in the analysis to predict more realistic tiltrotor whirl flutter stability. It will increase the number of degrees of freedom in the analysis from the present four to nine. Unsteady aerodynamic effect will be maintained in the new 9-DOF analytical model in which three flapping (β_0, β_{1c}, and β_{1s}), three lagging (ζ_0, ζ_{1c}, and ζ_{1s}), and three wing modes (torsion, vertical bending, and chordwise bending) are included.

Acknowledgment

This work was supported partially by grant No. R01-2005-000-10059-0 from the Basic Research Program of the Korea Science & Engineering Foundation. It was also supported by Korea Science & Engineering Foundation through the Joint Research Program (Grant No. F01-2007-000-10077-0).

References

[1] E. S. Taylor and K. A. Browne, Vibration Isolation of Aircraft Power Plants, *Journal of the Aeronautical Sciences*, 6 (2) (1938) 43-49.

[2] W. E. Jr. Hall, Prop-Rotor Stability at High Advance Ratios, *Journal of the American Helicopter Society*, 11 (2) (1966) 11-26.

[3] R. G. Kvaternik and J. S. Kohn, *An Experimental and Analytical Investigation of Proprotor Whirl Flutter*, NASA Technical Paper-1047, (1977).

[4] C. W. Acree et al., *Rotor Design Options for Improving XV-15 Whirl-Flutter Stability Margins*, NASA Technical Paper-2004-212262, (2004).

[5] M. W. Nixon et al., Tiltrotor Vibration Reduction Through Higher Harmonic Control, *American Helicopter Society 53rd Annual Forum* [CD-ROM], Virginia Beach, Virginia, April 29-May 1, (1997).

[6] R. G. Kvaternik et al., An Experimental Evaluation of Generalized Predictive Control for Tiltrotor Aeroelastic Stability Augmentation in Airplane Mode of Flight, *American Helicopter Society 57th Annual Forum* [CD-ROM], Washington, DC, May 9-11, (2001).

[7] R. Singh and F. Gandhi, Wing Flaperon and Swashplate Control for Whirl flutter Stability Aug-

mentation of a Soft in-plane Tiltrotor, *The 31st European Rotorcraft Forum* [CD-ROM], Florence, Italy, Sept. 13-15, (2005).

[8] W. Johnson, Dynamics of Tilting Proprotor Aircraft in Cruise Flight, NASA Technical Note D-7677, (1974).

[9] R. L. Bisplinghoff, H. Ashley and R. L. Halfman, *Aeroelasticity*, Dover, New York, (1996), Chap. 6.

[10] J. M. Greenberg, *Sinusoidal Motion in Pulsating Stream*, NASA TN 1326, (1947).

[11] C. E. S. Cesnik, *16.242 Aeroelasticity*, Lecture Note, Department of Aeronautics and Astronautics, Massachusetts Institute of Technology, Cambridge, Massachusetts, (1998).

[12] M. A. H. Dinyavari and P. P. Friedmann, Application of Time-Domain Unsteady Aerodynamics to Rotary-Wing Aeroelasticity, *AIAA Journal*, 24 (9), (1986) 1424-1432.

[13] R. T. Jones, *The Unsteady Lift of a Wing of Finite Aspect Ratio*, NACA Report 681, (1940).

[14] R. T. Jones, *Operational Treatment of the Nonuniform Lift Theory to Airplane Dynamics*, NACA TN 667, (1938).

[15] P. P. Friedmann and L. H. Robinson, Influence of Unsteady Aerodynamics on Rotor Blade Aeroelastic Stability and Response, *AIAA Journal,* 28 (10) (1990) 1806-1812.

[16] W. Johnson, *Analytical Modeling for Tilting Proprotor Aircraft Dynamics Including Blade Torsion and Coupled Bending modes, and Conversion Mode Operation*, NASA TM X-62, 369 (1974).

[17] M. W. Nixon, *Aeroelastic Response and Stability of Tiltrotors with Elastically-Coupled Composite Rotor Blades*, Ph.D. Thesis, University of Maryland, (1993).

[18] E. L. Hathaway, *Active and Passive Techniques for Tiltrotor Aeroelastic Stability Augmentation*, Ph.D. Thesis, The Graduate School College of Engineering, The Pennsylvania State University, (2005).

[19] D. M. Maisel et al., *The History of the XV-15 Tilt Rotor Research Aircraft: From Concept to Flight*, NASA SP-2000-4517, (2000).

Taeseong Kim received his B.S. in Aerospace Engineering from Korea Aviation University, Korea, in 2004. He then received his M.S. and Ph.D. degrees from Seoul National University in 2006 and 2009, respectively. Dr. Kim is currently a Research Scientist at Wind Energy Division at Risø National Laboratory for Sustainable Energy in Roskilde, Denmark. His research interests include aeroelasticity, wind turbine dynamics, rotorcraft dynamics, and structural dynamics.

SangJoon Shin received S.M. and Ph.D. degrees in Aeronautics and Astronautics from Massachusetts Institute of Technology in 1999 and 2001, respectively. From 1991 – 1996, he worked at the Helicopter Systems Department, Korean Agency for Defense Development. From 2001-2003, he worked at the Department of Aerospace Engineering, University of Michigan, Ann Arbor. Since 2003, he has been a professor at the School of Mechanical and Aerospace Engineering in Seoul National University. His research interests include aeroelasticty, rotorcraft dynamics, and smart structures.

Taehyoun Kim earned a Ph.D. in Aeronautics and Astronautics from Massachusetts Institute of Technology in 1992. Since 1996 he has worked in Loads and Dynamics Group of Boeing Commercial Aircraft, Seattle, Washington, USA. Prior to joining the Boeing Company he worked in Computational Mechanics Laboratory at Georgia Institute of Technology. Since 2005, he has been teaching a short course, "Computational Methods in Aeroelasticity" at SDM Conference, Boeing Ed Wells, National Aerospace Laboratory in India, and NASA Langley. Dr. Kim's specialties are aeroservoelasticity/structural dynamics, computational and experimental methods in aeroelasticity, system identification and model reduction of large-scaled dynamic systems, and composite structures.